resources

MDPI

Article

Combined Remediation towards Cadmium–Arsenic-Contaminated Soil via Phytoremediation and Stabilization

Chenxu Zhang [1,2,3], Jiamei Wu [1,2,3] and Jian Cao [1,2,3,*]

[1] School of Minerals Processing and Bioengineering, Central South University, Changsha 410083, China
[2] Key Laboratory of Hunan Province for Clean and Efficient Utilization of Strategic Calcium-Containing Mineral Resources, Central South University, Changsha 410083, China
[3] Hunan International Joint Research Center for Efficient and Clean Utilization of Critical Metal Mineral Resources, Central South University, Changsha 410083, China
* Correspondence: caojianlzu@163.com

Abstract: Using a phytoremediation technique for soil remediation usually takes many years, which increases the risk that heavy metals spread into the environment during the project period. Currently, the combined remediation technique (phytoremediation and stabilization) is known as the solution to reduce this risk. In this study, the combined remediation of cadmium–arsenic-contaminated soil via phytoremediation and stabilization was studied. The pot experiment was carried out using modified fly ash (MFA) and solid waste material (steel slag (SS): pyrolusite (PY): ferrous sulfide (FS) = 1:2:8) as stabilization materials and *Bidens pilosa* as the accumulative plant. The characteristics of *B. pilosa*, including its water content, biomass, root length, plant height, and heavy metal content, were obtained after harvesting, and the reduction rate of the bioavailability of Cd and As and their physico-chemical properties, including the pH, Eh, and Ec values of the soil, were also measured. The remediation effect was evaluated according to the above indexes, and the mechanism of combined remediation was studied through the FTIR, XRD, and XPS analyses. These experiments have shown that adding an appropriate amount of MFA can enhance the absorption of heavy metals by plants in the soil and reduce the bioavailability of heavy metals in contaminated soil. In addition, the mechanism study revealed that Cd^{2+}/$Cd(OH)^{+}$ was easily adsorbed on Si-OH and MnOOH, while AsO_4^{3-} was more easily adsorbed on Fe-OH and Al-OH.

Keywords: heavy metal; modified fly ash; phyto-extraction; soil remediation; solidification

Citation: Zhang, C.; Wu, J.; Cao, J. Combined Remediation towards Cadmium–Arsenic-Contaminated Soil via Phytoremediation and Stabilization. *Resources* **2023**, *12*, 109. https://doi.org/10.3390/resources12090109

Academic Editor: Benjamin McLellan

Received: 29 July 2023
Revised: 1 September 2023
Accepted: 6 September 2023
Published: 7 September 2023

1. Introduction

Cadmium and arsenic heavy metal pollution rank among the top five in the world [1]. The pollution of cadmium and arsenic towards the soil has been caused by extensive mineral mining, separating, smelting, and deep processing, which result in growing serious environmental problems [2]. Cadmium and arsenic pollution not only impair soil fertility and crop yield, but also cause serious harm to human health through their accumulation in the food chain [3].

The half-life of cadmium in the human body is 30 years, and the long-term accumulation of cadmium obviously damages the kidney organs, inducing various diseases, such as proteinuria, glycosuria, kidney atrophy, and glomerulosclerosis [4]. Arsenic and relevant compounds are highly toxic, which have been recognized as a group I carcinogen by the International Agency for Research on Cancer (IARC) [5]. In addition, arsenic and relevant compounds have also been found to induce anemia and acute kidney failure [6]. As soil pollution by cadmium and arsenic generates a great number of potential dangers to human health, more and more attention has been paid to the soil remediation techniques for cadmium and arsenic pollution [7–11].

Phytoremediation technology is an eco-friendly remediation technology developed in recent years [12–15]. Hyper-accumulators absorb and enrich heavy metals from the

contaminated soil during the growth process, promoting the transformation of heavy metals to a low toxicity state, and remove the heavy metals enriched in plants out of the polluted soil [16,17]. In this way, heavy metal pollutants in the polluted soil are continuously removed via the repeated planting and harvesting [18]. However, phytoremediation technology generally utilizes a long treatment period, and pollutants can easily be dispersed during the phytoremediation process (mainly caused by the activation of heavy metals by the vital activity of plants and microbiology), especially in the case of the cadmium and arsenic pollutants [19]. In consequence, safer and controllable soil remediation technology is urgently needed.

Stabilization remediation technology is one of the most common remediation methods in soil heavy metal remediation research [20]. By adding curing agents or stabilizers to contaminated soil, the physical and chemical properties of the contaminated soil could be adjusted, and the toxicity, biological availability, and migration ability of the heavy metals in the soil could also be effectively reduced [21]. The advantages of stabilization remediation technology can compensate the defects of phytoremediation technology, and as a result, the combined remediation of phytoremediation and stabilization technology is gradually becoming a research hotspot.

He et al. utilized *Solanum nigrum* L. and polyaspartate to remediate lead contaminated soil, and their results demonstrated that polyaspartate decreased the concentration of available Pb in metal-polluted soils to about 69.0% [22]. Guo et al. studied the combined remediation of copper-lead contaminated soil using native plants and sludge residues under a high-temperature treatment, and their results showed that the stable state content of the heavy metals copper (Cu) and lead (Pb) were effectively increased [23]. However, until now, there few studies available that report the combined remediation of phytoremediation and stabilization technology towards cadmium–arsenic-contaminated soil.

In our preliminary study, the combined remediation of the pioneer plant *B. pilosa* and mixed stabilization materials (steel slag: manganese ore: $FeSO_4$ = 1:2:8) was particularly effective in reducing the bioavailable state of cadmium by about 97.73%, but the reduction in the bioavailable state of arsenic was indistinctive [24]. The objective of this study was to study the combined remediation effect of potential plants and novel solid waste materials. In this work, a modified fly ash material was proven to be highly efficient for the reduction in the bioavailable states of arsenic in solids. Incorporating this modified fly ash material into previous combined remediation techniques, the bioavailable states of cadmium and arsenic in solids were able to be significantly reduced at the same time.

2. Materials and Methods

2.1. Characteristics of the Contaminated Soil

The experimental soil was collected from the affected area of an arsenic slag smelter (24.46° N, 111.28° E, 173 m a.s.l) in Zhongshan County, Guangxi, South China. The soil used in this study was taken from farmland soil and classified as anthrosols, based on the WBR classification. In order to evaluate the pollution degree of heavy metals in soil, the Nemerow method, an important pollution index method, was adopted. The Pi values of various heavy metal elements were calculated according to the Nemerow method, and the soil pollution degree was classified according to the Pi values [25]. The results are shown in Table 1. Following calculation and comparison, it was found that the pollution of Cd and As in the soil is relatively serious. In this affected area, heavy metal pollution was serious, but different wild plants grew, including *B. pilosa*, *Boehmeria nivea*, *Eremochloa ciliaris*, and *Leersia hexandra Swartz*, among which *B. pilosa* was the most abundant.

The sampling method of the soil samples was described by Barbara [26]. Thirty soil samples were collected from 0–20 cm of topsoil with a stainless steel shovel. The soil samples were mixed well and collected in a suitable-sized sample bag. Before use, the soil was dried for 24 h and finally passed through a screen with a diameter of 2 mm. The bioavailable heavy metals cadmium and arsenic were extracted from buffered DTPA solution and $NaHCO_3$ solution, respectively. Finally, the content of heavy metals was

determined using inductively coupled plasma mass spectrometry (ICP-MS) (NEXION 2000, Parkin Elmer Healthy Technology Co., Ltd., Beijing, China).

Table 1. The heavy metal content and pollution characteristics of soil.

Soil Parameter	Value
Soil pH	6.25
Organic matter content ($mg \cdot kg^{-1}$)	13.5
Available N ($mg \cdot kg^{-1}$)	663
Available P ($mg \cdot kg^{-1}$)	360
Available K ($mg \cdot kg^{-1}$)	64
Cation exchange capacity ($meq \cdot 100g^{-1}$)	6.37
Total Cd ($mg \cdot kg^{-1}$)	0.38
Total As ($mg \cdot kg^{-1}$)	76.14

2.2. Experimental Design of Combined Remediation

B. pilosa was selected as the pioneer plant through the pre-pot experiment. Solid waste is a mixture of modified fly ash (MFA), steel slag (SS), pyrolusite (PY), and ferrous sulfate (FS). The main components of SS and PY are shown in Tables 2 and 3, respectively. The total amount of SS, PY, and FS was 5% of the soil amount (SS:PY:FS = 1:2:8), and the amount of MFA was 0–1% of the soil amount. FM is a single Fe-Mn material remediation group. PFM is the Fe-Mn material–plant combined remediation group. $PFMM_x$ is the Fe-Mn material–MFA–plant combined remediation group, with x representing the amount of MFA, such as 0.2 represents the addition of 0.2% MFA.

Table 2. Main components of steel slag.

Compound	CaO	Fe_2O_3	SiO_2	MgO	Al_2O_3	MnO	SO_3	P_2O_5	TiO_2
Content (%)	44.32	18.12	12.12	8.74	7.96	3.07	1.56	1.48	1.29

Table 3. Main components of pyrolusite.

Compound	SiO_2	MnO	Fe_2O_3	Al_2O_3	CaO	K_2O	MgO	P_2O_5	TiO_2
Content (%)	44.00	23.67	22.54	6.27	0.80	0.77	0.52	0.43	0.21

Polyethylene flowerpots (8.5×10^{-4} m^3) were used in this test. The contaminated soil and solid waste were evenly mixed and placed in a flower pot for two weeks. After stabilization, 0.2 g of plant seeds were planted in pots and repeated 3 times for each treatment group. The combined remediation pot experiment was carried out in the greenhouse for 60 days. Finally, the above- and below-ground parts of the plant were removed from the soil, and the stems and leaves were separated from the roots. The plants and soil samples were collected for further processing and analysis.

The modified fly ash was prepared according to the method of our previous research [27]. Firstly, the magnetic fly ash was prepared via ferro-salt coprecipitation through ultrasonic stirring of fly ash + ferric salt in a 50 °C water bath device. Then, the magnetic fly ash and 3, 4-dihydroxybenzaldehyde were heated and stirred under an ethanol system at 70 °C for 2 h, following which melamine was added to the hot DMSO solution for 1 h. Finally, the ethanol in the previous system was evaporated using a rotary evaporator, and the DMSO solution of citric acid and the product were stirred at 80 °C for 1 h, washed, filtered, and dried, and the final modified fly ash (MFA) was obtained. The resulting XRD patterns of the original fly ash (FA) and the MFA are shown in Figure 1, and the main components of FA are shown in Table 4.

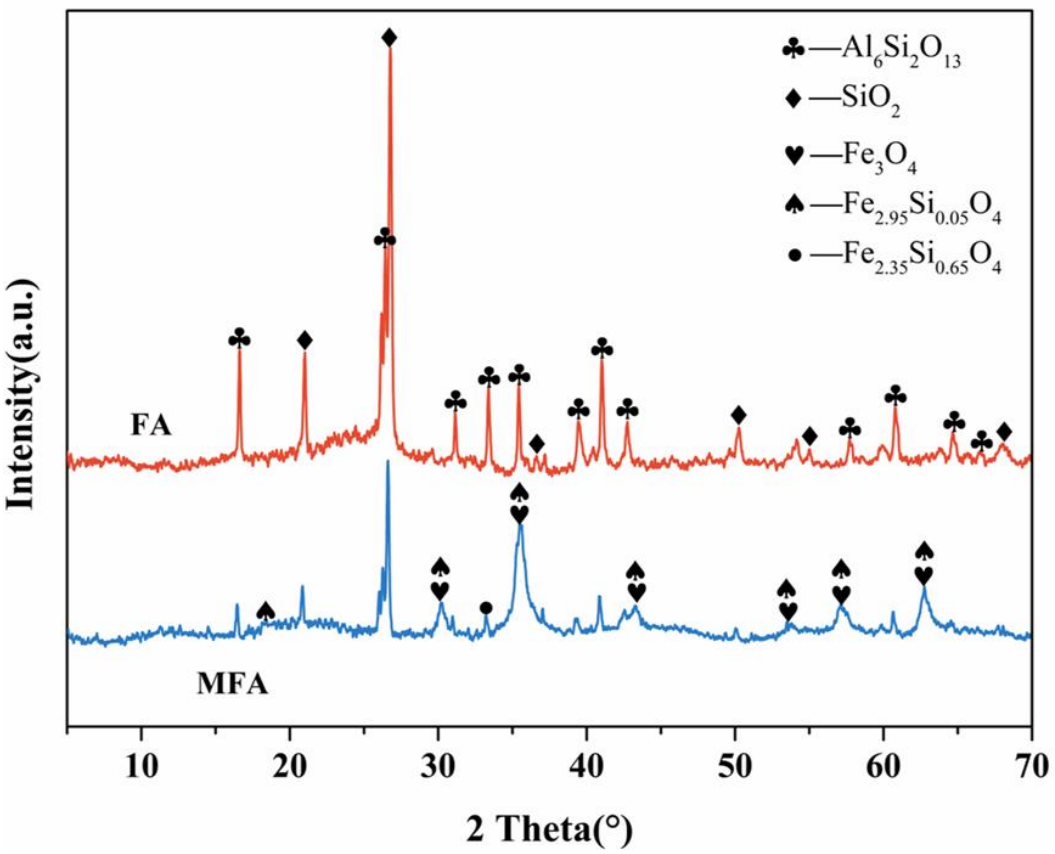

Figure 1. XRD patterns of fly ash (FA) and modified fly ash (MFA).

Table 4. The heavy metal content and pollution characteristics of soil.

Compound	SiO_2	Al_2O_3	Fe_2O_3	CaO	K_2O	TiO_2	Na_2O	MgO	SO_3
Content (%)	62.30	26.27	3.50	2.54	2.17	1.02	0.67	0.64	0.52

2.3. Analysis Method of Plant Samples

After collecting the plants, the wet weight and dry weight of the plants were measured using an electronic balance to calculate the water content and the biomass of the plants. A ruler was used to measure plant height.

The plants were dried to a constant weight and crushed into powder, and each part of the plants was digested according to the method described in the literature [22]; that is, 0.04 g of plant samples were added into each polytetrafluoroethylene crucible, and 8 mL of aqua regia was transferred into the crucible with a pipette, and then digested on the constant temperature electric heating plate in the fume hood (temperature: 150 °C). When there was about 3 mL of liquid left in the pot, the digestion temperature was lowered, the cover was lifted, and the crucible was shaken for digestion and desilication so that the digestion solution was clarified and no residue remained. After the crucible was taken off and cooled, the entire digestion solution was transferred to a 50 mL volumetric bottle. The inner wall of the crucible (cover) was then cleaned with deionized water 2–3 times, following which it was poured into the volumetric bottle and mixed well at a constant volume. The content of heavy metals in plants was measured using ICP-MS (NEXION 2000, Parkin Elmer Healthy Technology Co., Ltd., Beijing, China).

2.4. Analysis Method of Soil Samples

Th soil pH value was determined following the steps below. The soil was air-dried, reduced, crushed, and screened using a screen with a pore size of 2 mm. Pure water was

used as an extraction agent; the water-to-soil ratio was 2.5:1, and the mixture was oscillated on a constant temperature water bath oscillator for 2 min. After standing for 30 min, a portable pH meter was used for determination.

An ORP electrode was used to measure the redox potential of soil directly in the pot. Using a drill to punch a hole in the flower pot, the ORP electrode was directly inserted into the hole, and the value was recorded after the indicated number was stable.

Soil conductivity was determined following the steps below. The treated soil sample was taken and added with water at a ratio of 1:5 (m/v). The sample was oscillated on a constant temperature water bath oscillator at 20 °C and 180 r/min for 30 min, and then filtered after standing for 30 min. The filtrate was measured with an electrical conductivity meter.

The determination of total heavy metal content in soil was carried out in the following steps. A total of 0.1 g of a dry soil sample was passed through a 100-mesh nylon sieve and placed in a 50 mL polytetrafluoroethylene crucible, and 6 mL of aqua regia was transferred into the crucible with a pipette. The mixture was heated and kept boiling for 2 h. The mixture was cooled to room temperature and the extract was filtered using slow filter paper into a 50 mL bottle. A small amount of dilute nitric acid was used to clean the crucible and filter residue at least 3 times, and the lotion was collected into the volumetric bottle. The content of heavy metals in soil was measured using ICP-MS.

The content of bioavailable heavy metals in soil was determined in the following steps. Soil and DTPA-$CaCl_2$-TEA extract or $NaHCO_3$ extract were added to the conical bottle at a ratio of 1:2 (m/v) and sealed with plastic wrap. At 20 °C, the oscillating frequency of 200 r/min was oscillated on a constant temperature water bath oscillator for 2 h. After centrifugation, the supernatant was filtered through a needle filter membrane for ICP-MS determination. The reduction rate of bioavailable heavy metals was defined as the following equation:

$$\eta\ (\%) = \frac{\eta_{\text{Before}} - \eta_{\text{After}}}{\eta_{\text{Before}}} \times 100$$

where η_{Before} is the content of bioavailable heavy metals in soil before combined remediation, and η_{After} is the content of bioavailable heavy metals in soil after combined remediation.

The biological enrichment coefficient (BF) of a plant is the ratio of a certain element content in the plant ($C_{\text{Plant}}/\text{mg}\cdot\text{kg}^{-1}$) to a certain element content in the soil ($C_{\text{Soil}}/\text{mg}\cdot\text{kg}^{-1}$). The transport coefficient is the ratio of the element content of the above-ground part of the plant ($C_{\text{Plant shoot}}/\text{mg}\cdot\text{kg}^{-1}$) to the underground part ($C_{\text{Root}}/\text{mg}\cdot\text{kg}^{-1}$). These formulas are defined as:

$$\text{BF} = C_{\text{Plant}}/C_{\text{Soil}}$$

$$\text{TF} = C_{\text{Plant shoot}}/C_{\text{Root}}$$

3. Results and Discussion

3.1. Results of the Biological Properties of Plants and Heavy Metal Content in Plants

According to the status of plant growth in Figure 2, it can be seen that *B. pilosa* exhibited good adaptability to the stabilization materials added. However, with the increase in the amount of MFA added, the growth status of the plants gradually deteriorated. Moreover, the column diagram in Figure 2 showed that with the increased dosage of MFA, the biomass of the plants continued to decline; however, the moisture and plant height of the plants did not change much. When the amount of MFA was 0.4%, the growth status of *B. pilosa* was at its best; the plant biomass was 43.04 g/m^2, the plant height was 6.9 cm, the water content was 84.98%, and the leaves were normal.

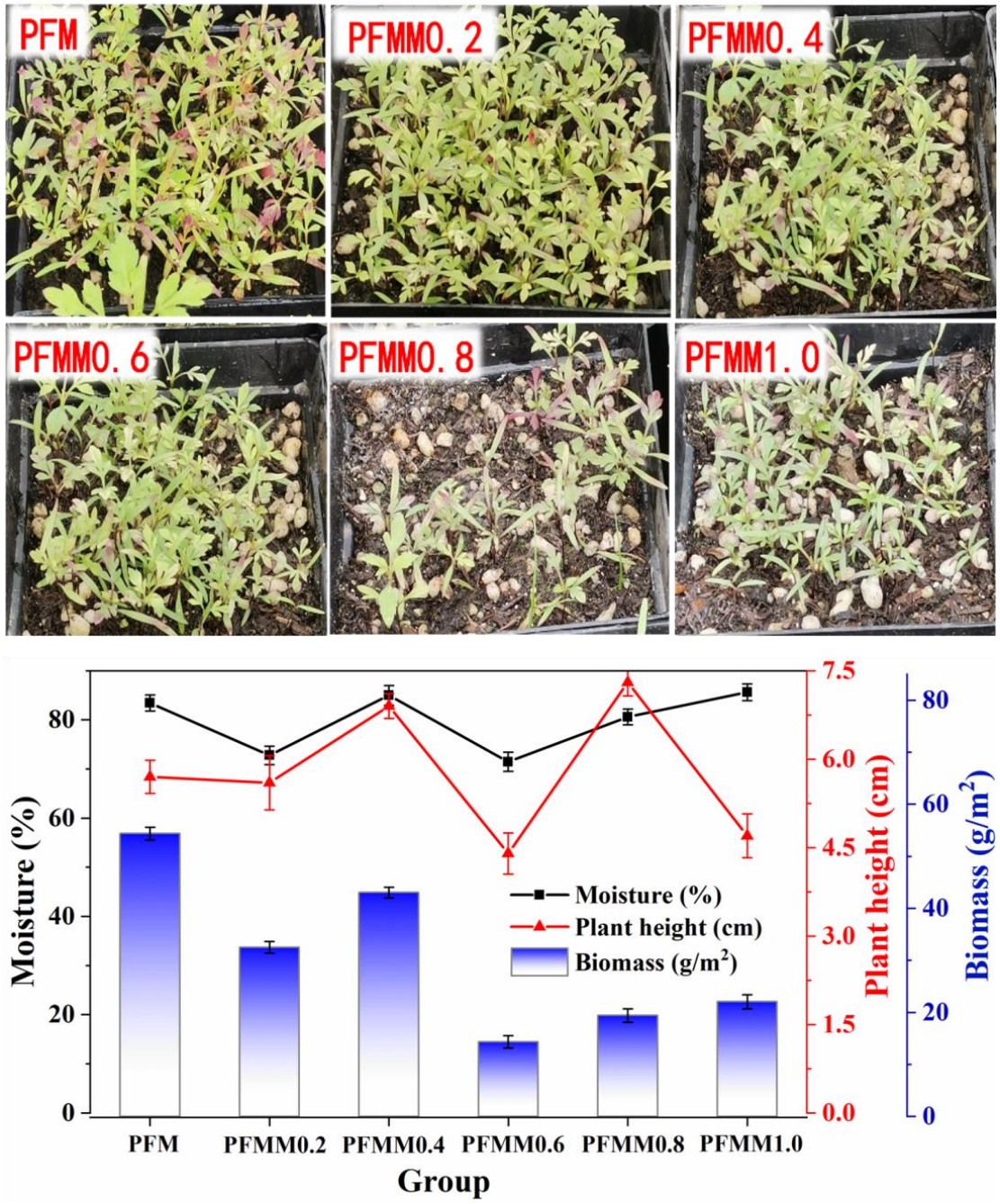

Figure 2. Growth status of *B. pilosa* under different MFA dosages.

Excessive fly ash material may affect the normal photosynthesis process of plants, thus affecting the accumulation of biomass. However, plant height and moisture may depend more on other factors, such as plant genetics and soil moisture, respectively.

Through screening plant growth along with comprehensive consideration of the biomass index, it was found that the optimal amount of MFA was 0.4%.

As can be seen from Figure 3a, with the increase in the amount of MFA, the contents of As and Cd in *B. pilosa* initially increased and then decreased. When the addition amount of MFA was 0.6%, the contents of As and Cd of *B. pilosa* were the highest. When 0.6% MFA was mixed with the Fe-Mn material, the content of Cd was increased, which promoted the extraction of Cd by plants. As can be seen from Figure 3b, when the amount of MFA increased, the Cd transport coefficient (TF) of *B. pilosa* first increased and then decreased. When 0.4% and 5% MFA were combined with the Fe-Mn material, the TFs for Cd and

As was at their highest, 1.158 and 0.594, respectively. The addition of MFA on the basis of PFM resulted in an increase in the Cd transport coefficient and a decrease in the As transport coefficient. As can be seen from Figure 3c,d, when different amounts of MFA were added, the bio-concentration factors of As and Cd of *B. pilosa* were reduced to different degrees. The maximum bio-concentration factor was 0.013 when the dosage was 0.8%. The enrichment coefficient of Cd was 8.16 when no MFA was added.

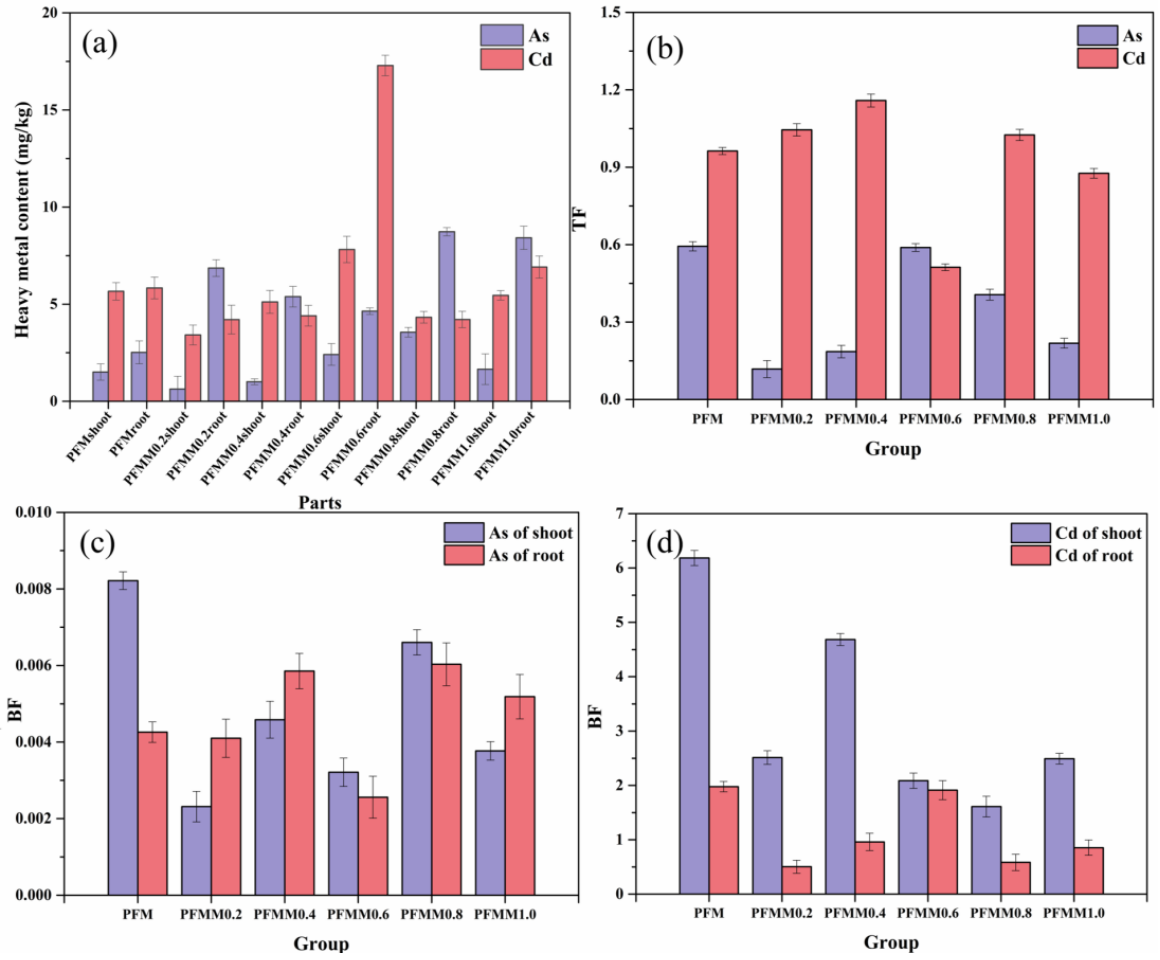

Figure 3. Heavy metal content (**a**), translocation factor (TF) (**b**), As bio-concentration factor (BF) (**c**), and Cd bio-concentration factor (BF) (**d**) of plants with different amounts of MFA.

In conclusion, when 0.6% of MFA was combined with the Fe-Mn material, the amounts of As and Cd extracted by *B. pilosa* were at their highest. When 0.4% and 0.6% MFA were combined with the Fe-Mn material, the TFs for Cd and As were at their highest, 1.158 and 0.589, respectively.

3.2. Results of the Physical and Chemical Properties of Soil and Heavy Metal Content in Soil

Figure 4 shows the contents of bioavailable cadmium and arsenic in soil with different MFA dosages. As the amount of MFA increased, the reduction rate of the bioavailable As increased, but that of Cd fluctuated. When the Fe-Mn material was combined with 0.8% MFA, the contents of bioavailable As and Cd were reduced by 60.56% and −21.29%, respectively. When the amount of MFA was increased to 1%, the availability of As and Cd was reduced by 11.52% and 69.43%, respectively. These results showed that only when the addition of MFA was greater than 1% did it have a promoting effect on the removal of As in the soil and a promoting effect on the removal of Cd.

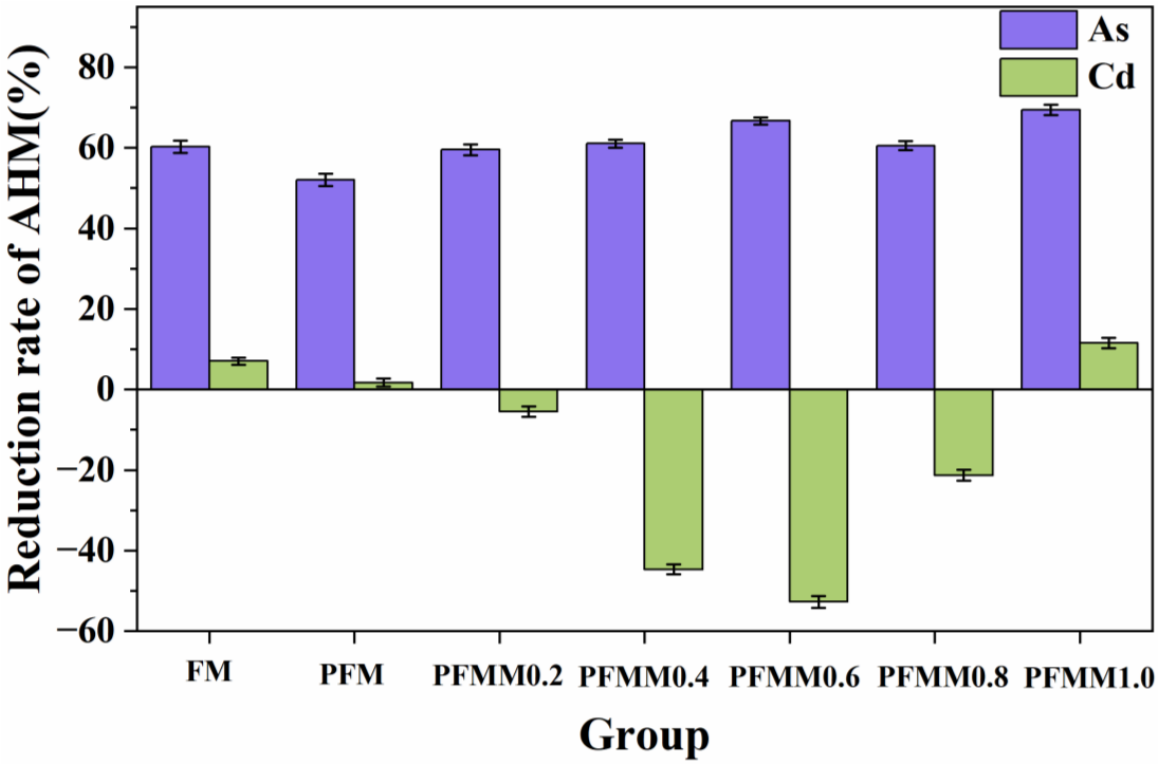

Figure 4. Contents of available heavy metals (AHMs) in soil with different MFA dosages.

By investigating the effect of reducing the bioavailable heavy metals, the best addition amount of MFA was at 0.8%.

As can be seen from Figure 5, the soil pH value first increased and then decreased with the increase in the amount of MFA. The overall pH of the soil was lower than that of the single Fe-Mn material remediation group, indicating that the addition of MFA resulted in a decreased soil pH value. The Eh value of the soil after remediation was still in the range of 100–550 mV, indicating that the soil maintained satisfactory permeability and moisture during remediation. After the addition of MFA, the Eh value of the soil decreased compared with the combined remediation group of Fe-Mn material and plants, indicating that the reduction state of the soil was enhanced, which was beneficial to the improvement of the soil properties [28]. With the increase in the amount of MFA, the soil Ec value first increased and then decreased, and reached the maximum value at 0.4% MFA, which was 1158 μs/cm. However, high electrical conductivity may cause damage to plant leaves, resulting in a reduction in plant yield. Moreover, it was found that when the amount of MFA was more than 0.6%, the biomass of plants decreased significantly, and the leaf redness appeared. Based on the transformation of the pH, Eh, and Ec values via dosage of the stabilization material, it can be concluded that the optimized dosage of MFA was 0.6% due to the minimal changes in the physical and chemical properties of the soil.

3.3. Study on the Combined Remediation Mechanism

As shown in Figure 6, in the infrared spectrum of steel slag (SS), the peaks observed at 1435.19 cm^{-1} and 875.13 cm^{-1} were the stretching vibration absorption peak of CaO and the bending vibration characteristic absorption peak of Fe-OH-Fe, respectively. The symmetric stretching vibration peak of (Al, Si) -O-Si was at 712.55 cm^{-1}, and the vibration absorption peak of the Si-O bond was at 518.01 cm^{-1} [29].

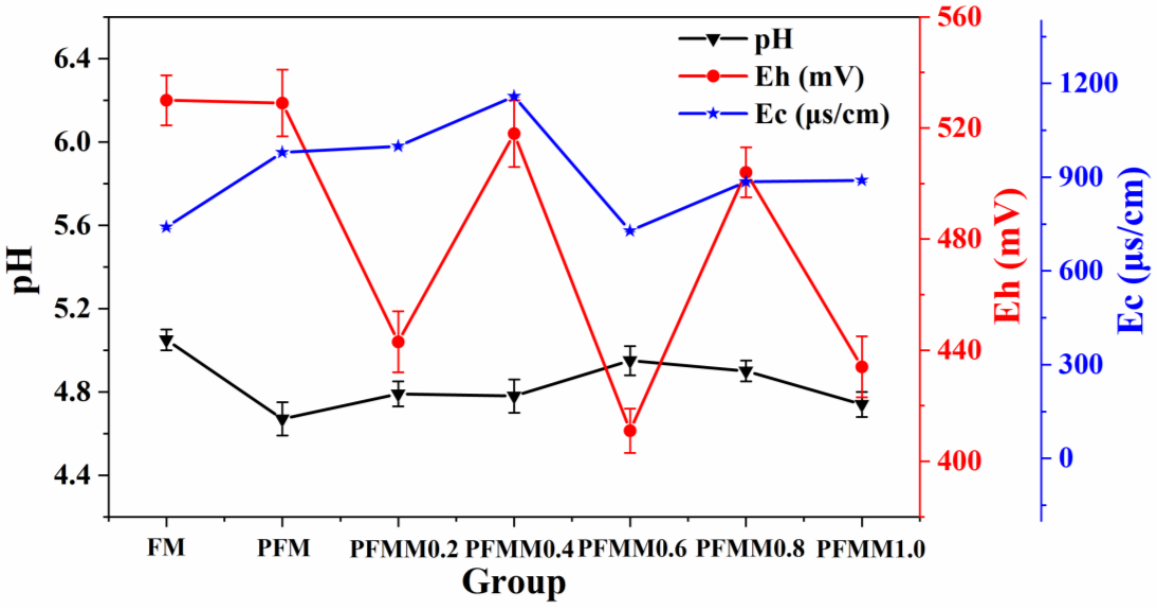

Figure 5. Physical and chemical properties of soil with different amounts of MFA.

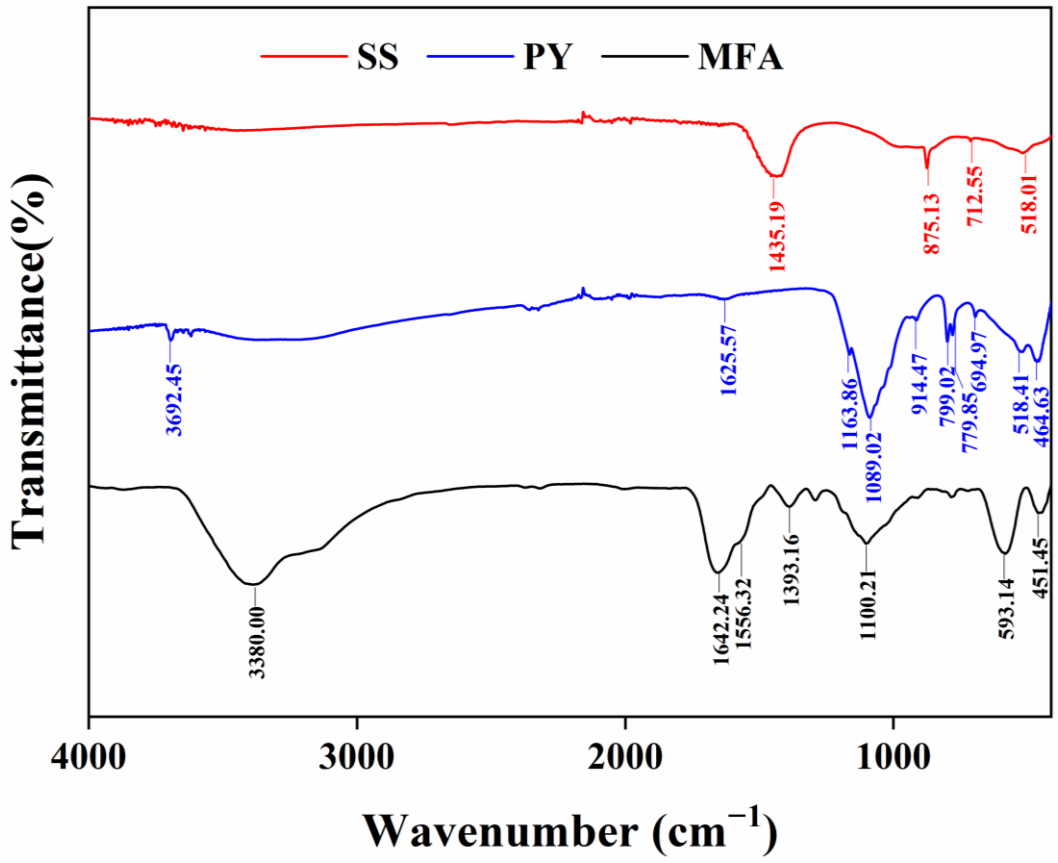

Figure 6. Infrared spectrogram of materials for stabilization.

In the infrared spectra of pyrolusite (PY), the peaks at 1625.57 cm^{-1} and 3692.45 cm^{-1} were both -OH peaks [30]. The characteristic peaks of silica appeared at 1089.02 cm^{-1} and 779.85 cm^{-1}, and the high intensity absorption peaks at 799.02 cm^{-1} were caused by the symmetric stretching vibration of Si-O-Si [31]. The peaks at 694.97 cm^{-1}, 518.41 cm^{-1}, and 464.43 cm^{-1} were determined to be the characteristic peaks of manganese oxide [32], while the peaks at 1163.86 cm^{-1} represented the vibration absorption peaks of MnOOH

of molybdenite [33]. The peak at 914.47 cm^{-1} was attributed to the stretching vibration absorption peak of Al-OH [34].

In the infrared spectra of MFA, the peaks observed at 451 cm^{-1} and 593 cm^{-1} were attributed to the Si-O/Al-O surface bending vibration and the Fe-O vibration absorption peaks, respectively [35,36]. The characteristic peak of silica appeared at about 1100 cm^{-1}, which belongs to the antisymmetric stretching vibration absorption peak of Si-O-Si [37]. In addition, the absorption peaks of organic functional groups were also observed at 1393.16 cm^{-1}, 1556.32 cm^{-1}, 1642.24 cm^{-1}, and 3380.00 cm^{-1}, which belonged to the tensile vibration of -COOH and C-N, the characteristic peak of C=N, and the characteristic absorption peak of -NH_2, respectively. Therefore, the presence of silicates and metal ions will solidify Cd and As in the soil, respectively

As can be seen from Figure 7, the infrared spectra of the original contaminated soil (YT) and the remediated soil (XFT) were different. The peaks of the two soil samples were highly consistent with those of kaolinite, including the peaks near 3696 cm^{-1}, 3620 cm^{-1}, 1032 cm^{-1}, 914 cm^{-1}, 694 cm^{-1}, 534 cm^{-1}, and 470 cm^{-1}, among which the -OH peaks near 3696 cm^{-1} and 3620 cm^{-1} indicated that the soil also contains polyaqueous kaolinite [38]. In addition, absorption peaks also appeared at 3445 cm^{-1}, 1635 cm^{-1}, and 796 cm^{-1}, which belong to the stretching vibration of structural water and free water-OH, the bending vibration of free water-OH, and the symmetric stretching vibration of the Si-O-Si bond [29].

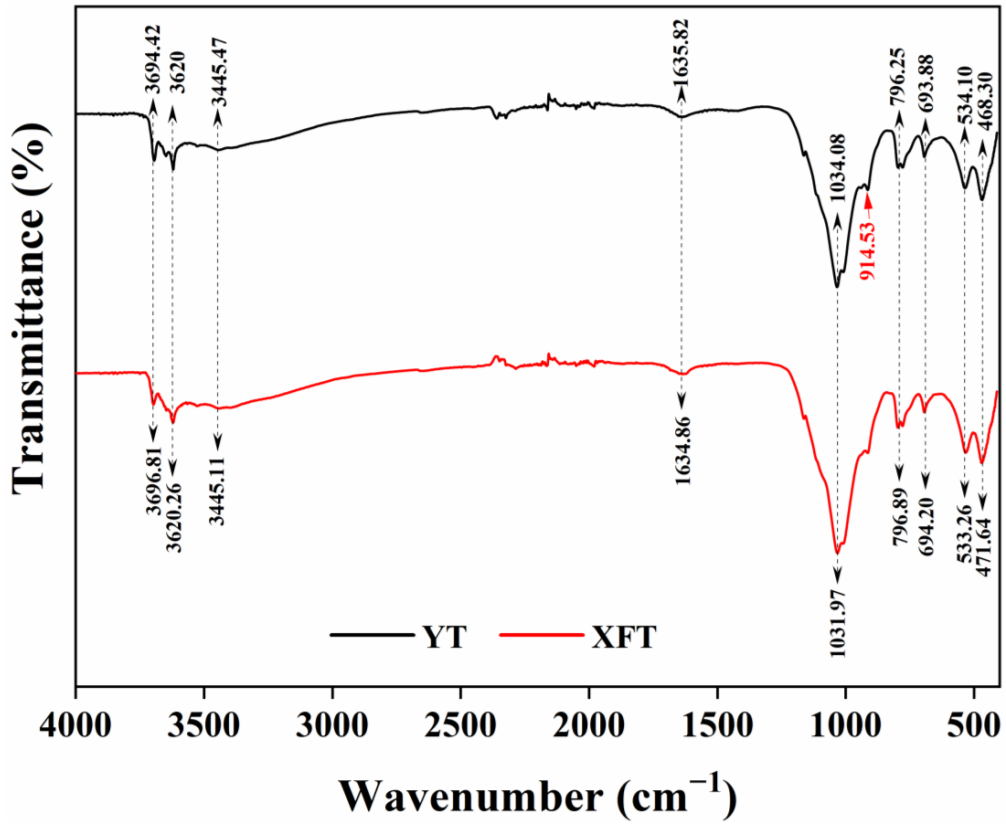

Figure 7. Infrared spectrogram of contaminated soil before and after remediation.

Combined with the infrared spectra in Figures 6 and 7, it can be seen that after the combined remediation of the stabilization material (Fe-Mn material + MFA) and plants, the peaks of Al-OH, -NH_2, C-N, CaO, -COOH, MnOOH, Fe-OH-Fe, (Al, Si) -O-Si, Fe-O, and manganese oxide in the contaminated soil disappeared, indicating that these peaks were involved in the process of stabilizing cadmium and arsenic. The complexation/chelation of the organic functional groups, such as -NH_2, C-N, and -COOH with Cd^{2+}, was determined to be consistent with the action mechanism of MFA in aqueous solution. Al-OH, CaO,

MnOOH, Fe-OH-Fe, (Al, Si) -O-Si, Fe-O, and manganese oxide may have an adsorption, double salt effect, isographic effect, or REDOX reaction with heavy metals.

As can be seen from Figure 8, the original contaminated soil only contains two minerals: quartz (SiO_2) and kaolinite ($Al_4(Si_4O_{10})(OH)_8$). It can be seen from the literature that steel slag contained feldspar granite (Ca_2SiO_4), pontenite (FeO), calcium aluminate ($12CaO{\cdot}7Al_2O_3$), black calcium calcium iron ($Ca_2Fe_2O_5$), calcium hydroxide ($Ca(OH)_2$), and other mineral phases [39]. Pyrolusite contains quartz (SiO_2), manganese dioxide (MnO_2), olivine ($(Fe, Mn)_2SiO_4$), and other mineral phases [40]. The XRD test result in Figure 1 showed that the main mineral phases of MFA are quartz (SiO_2), mullite ($Al_6Si_2O_{13}$), magnetite (Fe_3O_4), and ferric oxide silicon. After adding the Fe-Mn material, the mineral facies of the soil were added mica ($KAl_2(AlSi_3O_{10})(OH)_2$), gypsum ($CaSO_4{\cdot}2H_2O$), and feldspar ($Or_xAb_yAn_z$ (x + y + z = 100), with Or, Ab, and An representing $KAlSi_3O_8$, $NaAlSi_3O_8$, and $CaAl_2Si_2O_8$, respectively). This was due to the hydration reaction between the oxide in the solid waste material and calcium hydroxide, with the reaction equation being as follows [41]:

$$SiO_2 + Ca(OH)_2 + nH_2O \rightarrow CaO{\cdot}SiO_2{\cdot}(n + 1)\ H_2O \quad (1)$$

$$Al_2O_3 + Ca(OH)_2 + nH_2O \rightarrow CaO{\cdot}Al_2O_3{\cdot}(n + 1)\ H_2O \quad (2)$$

$$3Ca(OH)_2 + 3CaSO_4 + Al_2O_3 + nH_2O \rightarrow AFt \quad (3)$$

$$2[2CaO{\cdot}SiO_2] + 6H_2O \rightarrow \text{calcium silicate hydrate (CSH)} + 3Ca(OH)_2 \quad (4)$$

$$Ca(OH)_2 + Al_2O_3 \rightarrow \text{calcium aluminate hydrate (CAH)} \quad (5)$$

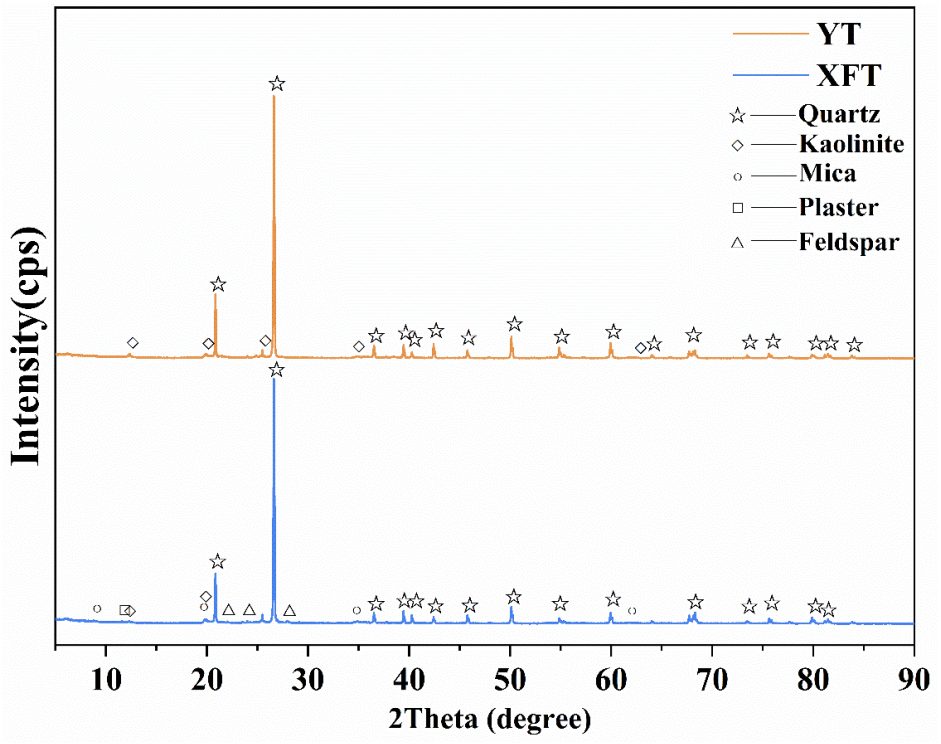

Figure 8. XRD spectrum of contaminated soil before (YT) and after (XFT) remediation.

The resulting calcium aluminate hydrate (C-A-H), calcium silicate hydrate (C-S-H), and ettringite (AFt) can enhance the fixation of cadmium ions through physical encapsulation or isotropy between Ca^{2+} and Cd^{2+} [42,43].

Figure 9 showed the peaks of the elements Fe, Mn, O, Cd, As, S, Ca, C, and N in the soil. The results showed that the peaks of N KLL, Fe 2s, Cd 3p1, Cd 3p3, Ca 2s, MN-3s, and MN-3p in the soil after remediation disappeared. After analysis, it was found that the peak strengths of Si2p at C1s, O1s, and 102 eV and Al2p at 74 eV were weakened, indicating that the above elements participated in the stabilization process of Cd and As, and the peak strengths of Si2p and Al2p were weakened as they participated in the hydration reaction. Therefore, in order to further judge the chemical changes of each element, XPS fine spectrum analysis was performed on the elements Cd, As, Fe, C, and O of the soil before and after remediation, and the results were shown in Figures 10 and 11.

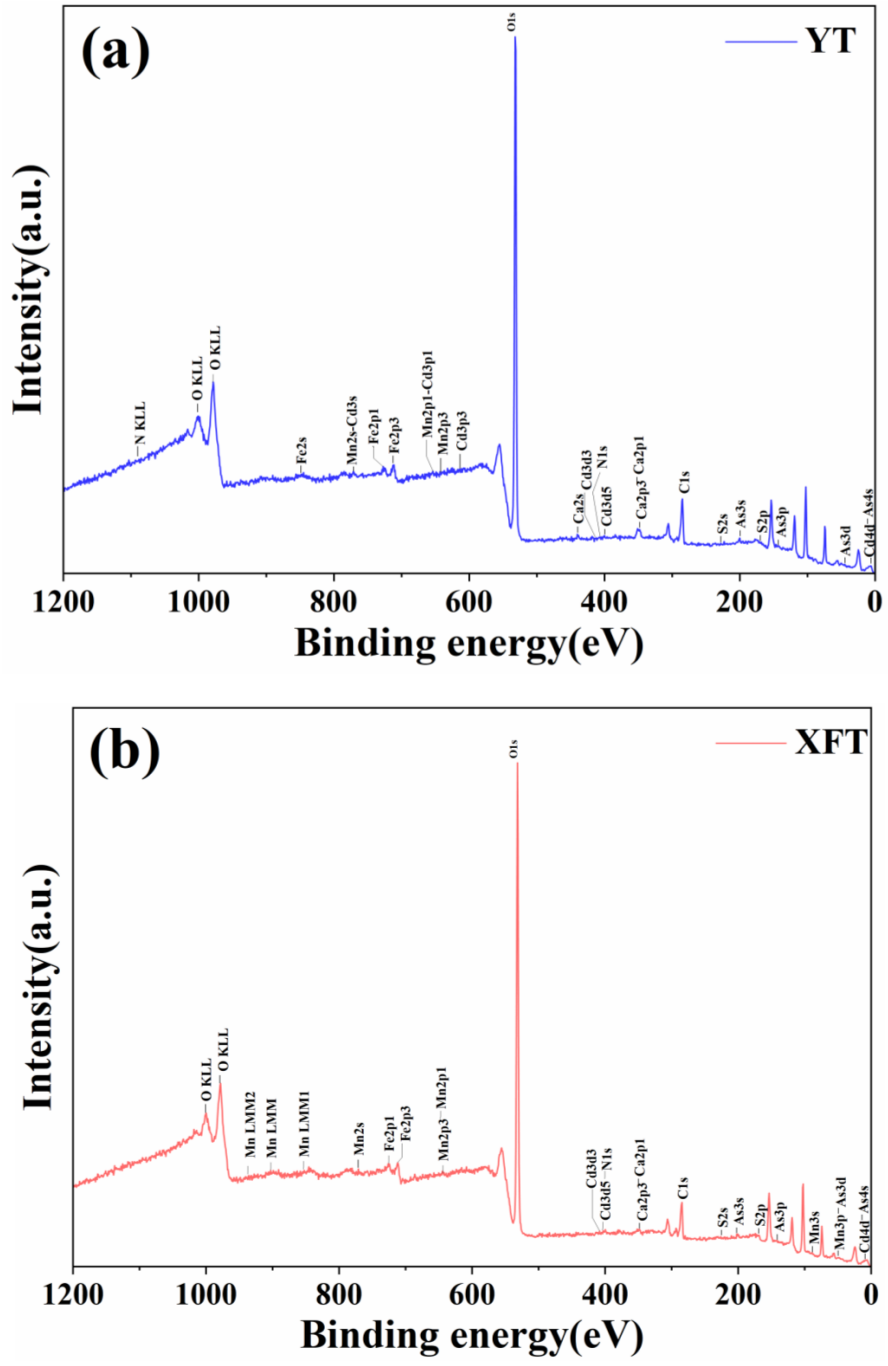

Figure 9. XPS full spectrum of contaminated soil before (**a**) and afte (**b**) remediation.

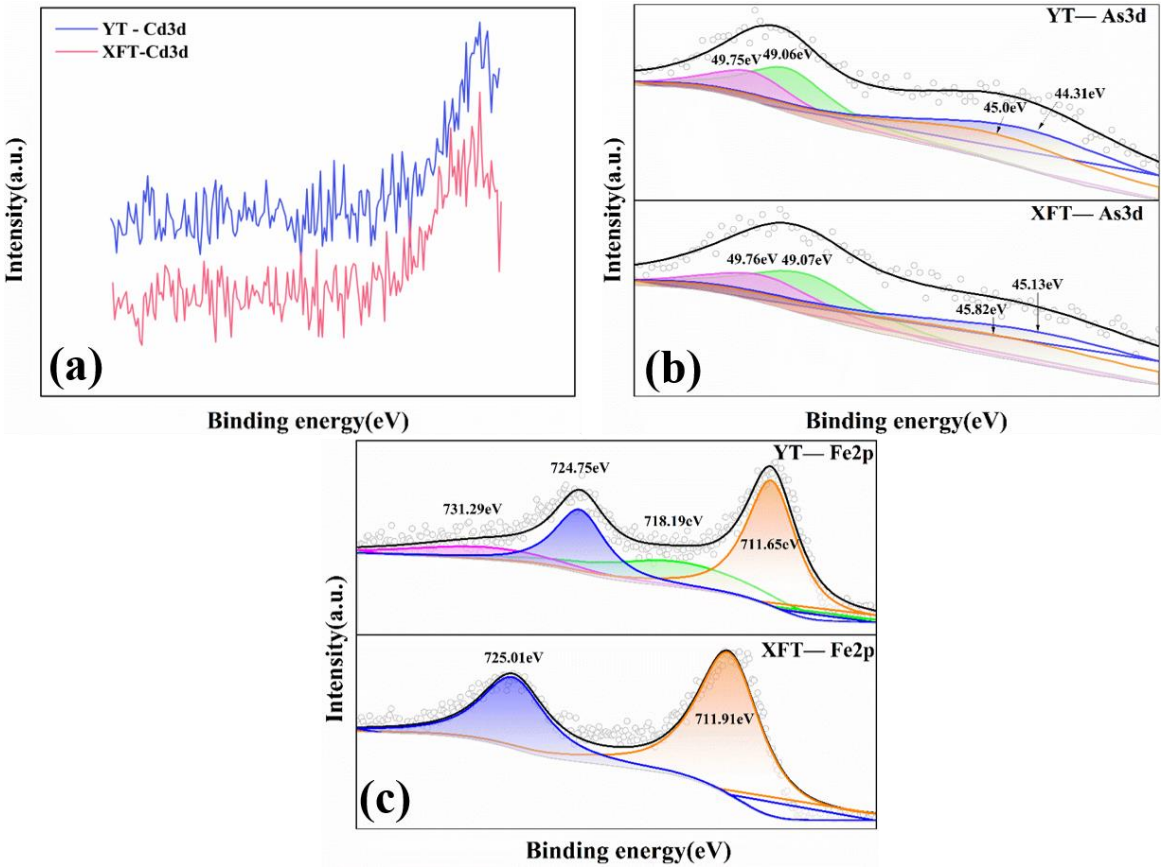

Figure 10. Cd3d (**a**), As3d (**b**), and Fe2p (**c**) XPS spectra of contaminated soil before (YT) and after (XFT) remediation.

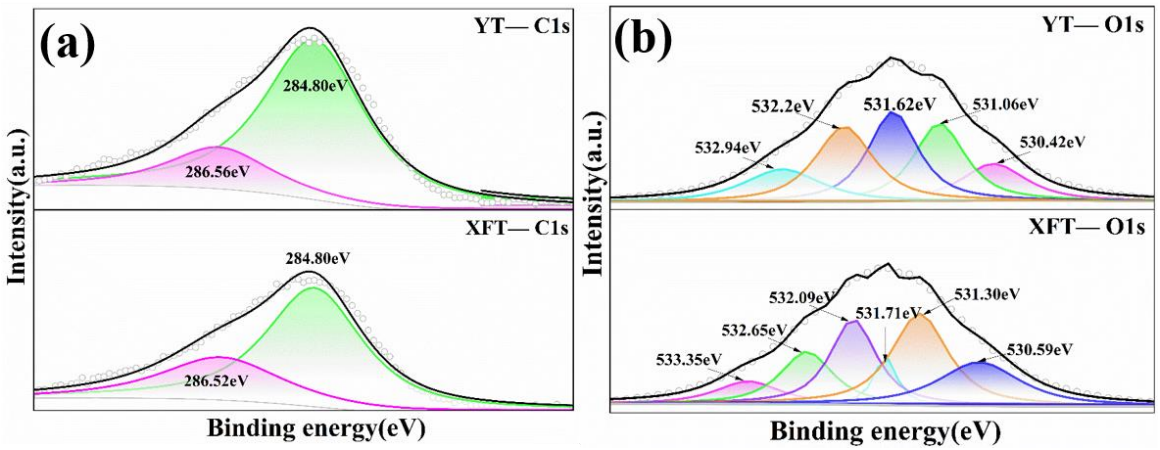

Figure 11. Narrow XPS spectra of C1s (**a**) and O1s (**b**) before and after remediation of contaminated soil.

Figure 10a displays the Cd3d XPS spectra before and after soil remediation. Since the content of Cd in the soil is less than 5%, it was impossible to carry out fine spectrum fitting analysis. As can be seen from Figure 10a, the peak of Cd3d was moving and the peak area was increasing after remediation. This was due to the plant root exudates (such as organic acids and carboxylates) increasing the bioavailability of Cd. The acid-soluble and water-soluble Cd formed a complex with the organic acids in the soil, which facilitates the absorption of cadmium by the plant roots, which is then released into the xylem and finally transferred to the abovementioned part [44].

The As3d-binding energies of As(V) and As(III) in arsenic oxides are shown in Figure 10b and were 49.06–49.76 eV and 44.31–45.82 eV, respectively [45]. As can be seen from the high-resolution spectrum of As3d, the binding energy of As(III) in the soil increased and the peak area decreased, while the binding energy of As(V) increased slightly and the peak area increased, indicating that As(III) and other substances underwent REDOX reactions to form As(V).

Figure 10c shows the Cd3d XPS spectra before and after soil remediation. According to the XPS Handbook, 711.65 eV was the peak of FeOOH, 724.75 eV was the peak of Fe(III) oxide, and 718.19 and 731.29 eV were the satellite peaks of Fe(III). The disappearance of the satellite peak of Fe(III) after remediation may be due to a small part of Fe(III) being reduced to Fe(II). Due to the REDOX properties of the Fe and Mn elements, and the oxidation of Fe(III) being weaker than that of Mn (IV), Mn (IV) first oxidized As (III) into As (V) with low toxicity and low migration, following which adsorption or the co-precipitation reaction occurred on the surface of iron oxide and manganese oxide to produce iron arsenate, manganese arsenate, and other substances, as shown in Equations (6) and (7) below [46,47]. This was the reason for the increase in the binding energy of the Fe(III) peak in soil after remediation.

$$MnO_2 + AsO_3^{3-} + 2H^+ \rightarrow Mn^{2+} + AsO_4^{3-} + H_2O \quad (6)$$

$$FeO(OH)(H_2O)_{1+x} + AsO_4^{3-} \rightarrow AsO_4^{3-} \cdot FeO(OH)(H_2O)_{1+x} \quad (7)$$

Figure 11a,b display the high-resolution maps of soil C1s and O1s before and after remediation, respectively. The peak at 286.56 eV corresponded to either the C=O peak or the carbon oxide generated by the surface species in contact with CO_2 [48]. After remediation, the peak value decreased and the peak area increased, indicating that the carboxylate increased in the soil after remediation and formed a complex with heavy metal ions, which may be the role of small molecular organic acids and carboxylates secreted by plant roots.

Only five peaks were detected in the O1s high-resolution spectrum of the original soil (Figure 11b), and one new peak was added in the remediated soil. A 530.42 eV value was obtained as the peak of the M-O metal oxide (M may be Fe, Al, Ca, or Mn) [49]. After remediation, the binding energy of M-O increased by 0.17 eV, and the peak area increased somewhat. The increase in the peak area was due to the increase in the amount of metal oxide due to the addition of the solid waste material. The increase in the binding energy may be due to the abundant hydroxyl groups on the surface of metal oxides, which combine with As and Cd to form stable outer and inner surface complexes. The obtained values 531.06 eV, 531.62 eV, and 532.2 eV correspond to the Si-O-M, Si-OH, and C-O peaks, respectively [50]. After remediation, the binding energy of Si-O-M increased by 0.24 eV, and the peak area increased. The binding energy of the Si-OH peak increased by 0.09 eV, and the peak area significantly decreased. This indicated that a large number of hydroxyl groups on the surface of SiO_2 combine with metal ions to form Si-O-M bonds, which may contain the precipitation mechanism of cadmium ions, as shown in equation 8. The obtained value of 532.94 eV belongs to the Si-O-Al peak; the binding energy decreased by 0.29 eV after remediation, and the peak area increased due to the hydroxyl group on the newly added silicon oxide reacting with aluminum oxide in the material. Fewer electrons enhanced the reduced states of Si and O, leading to the formation of more Si-O-Al bonds. The peak at the added 533.35 eV was carbonate (MCO_3), as shown in Equations (9) and (10):

$$Cd^{2+} + SiO_2 + 2OH^- + n\ H_2O \rightarrow SiO_2CdO \cdot (n + 2)H_2O \quad (8)$$

$$2OH^- + CO_2 \rightarrow CO_3^{2-} \quad (9)$$

$$Cd^{2+} + CO_3^{2-} \rightarrow CdCO_3\downarrow \quad (10)$$

In addition, the PI value (isoelectric point) also affected the adsorption between the metal ions and oxides. The known PI values for Fe_2O_3, FeOOH, Al_2O_3, MnO_2, and SiO_2 are 8.4–9, 8.5, 8.2, 4.8, and 3, respectively. Therefore, under all pH conditions, the number of negative charge sites (hydroxyl groups) of the above oxides was ordered as SiO_2 > MnO_2 > Al_2O_3 > FeOOH > Fe_2O_3. Therefore, Cd^{2+}/$Cd(OH)^+$ was easily adsorbed on Si-OH and MnOOH, while AsO_4^{3-} was more easily adsorbed on Fe-OH and Al-OH [51].

4. Conclusions

In this study, the combined remediation of cadmium–arsenic-contaminated soil via phytoremediation (*B. pilosa*) and stabilization (Fe-Mn material + MFA) was studied, and the main conclusions are as follows:

(1) The addition of an appropriate amount of Fe-Mn material and MFA can promote plant growth, while too much MFA was adverse for plant growth.
(2) Fe-Mn material and MFA can improve the transport capacity of plants for As and Cd, respectively. In addition, the contents of As and Cd in the body of *B. pilosa* first increased and then decreased with the increase in the addition amount of MFA.
(3) The addition of MFA can help to remove As in the soil, while the addition of MFA can help to remove Cd under the addition amount being above 1%.
(4) The mechanism of stabilization material–plant combined remediation includes the adsorption and precipitation of heavy metal ions, isomorphic substitution, and chelation of organic acids in the plant roots. Cadmium and arsenic ions can be stabilized on the surface of different oxides via electrostatic attraction or precipitation formation.

Based on the application prospect of this study, *B. pilosa* exhibits high adaptability to the stabilization materials used, meaning that it has high potential in practical applications. This work may also be applied to Zhuzhou City of Hunan Province, Jiujiang County of Jiangxi Province, and Hezhang County of Guizhou Province in China, where heavy metal pollution is severe.

Author Contributions: Conceptualization, C.Z.; methodology, C.Z.; formal analysis, J.W.; investigation, C.Z. and J.W.; data curation, C.Z. and J.W.; writing—original draft preparation, C.Z. and J.W.; writing—review and editing, J.C.; supervision, J.C.; funding acquisition, J.C. All authors have read and agreed to the published version of the manuscript.

Funding: This work was supported by the National key Research and development program [2019YFC1803500]; the Science and Technology Innovation Program of Hunan Province [2022RC1039]; and the Natural Science Foundation of China [52004336, 52274287]; and the Comprehensive Survey Project for Ecological Restoration in Dongting Lake Wetland [DD20230478].

Data Availability Statement: Data are available from the authors upon reasonable request.

Conflicts of Interest: The authors declare no conflict of interest.

References

1. Mama, C.N.; Nnaji, C.C.; Igwe, O.; Ozioko, O.H.; Ezugwu, C.K.; Ugwuoke, I.J. Assessment of heavy metal pollution in soils: A case study of Nsukka metropolis. *Environ. Forensics* **2022**, *23*, 389–408. [CrossRef]
2. Wen, J.; Yan, C.Y.; Xing, L.; Wang, Q.; Yuan, L.; Hu, X.H. Simultaneous immobilization of As and Cd in a mining site soil using HDTMA-modified zeolite. *Environ. Sci. Pollut. Res.* **2021**, *28*, 9935–9945. [CrossRef] [PubMed]
3. Khan, S.I.; Ahmed, A.K.M.; Yunus, M.; Rahman, M.; Hore, S.K.; Vahter, M.; Wahed, M.A. Arsenic and Cadmium in Food-chain in Bangladesh—An Exploratory Study. *J. Health Popul. Nutr.* **2010**, *28*, 578–584. [CrossRef] [PubMed]
4. Ishizaki, M.; Suwazono, Y.; Kido, T.; Nishijo, M.; Honda, R.; Kobayashi, E.; Nogawa, K.; Nakagawa, H. Estimation of biological half-life of urinary cadmium in inhabitants after cessation of environmental cadmium pollution using a mixed linear model. *Food Addit. Contam. Part A-Chem.* **2015**, *32*, 1273–1276. [CrossRef] [PubMed]
5. Prakash, C.; Chhikara, S.; Kumar, V. Mitochondrial Dysfunction in Arsenic-Induced Hepatotoxicity: Pathogenic and Therapeutic Implications. *Biol. Trace Elem. Res.* **2022**, *200*, 261–270. [CrossRef]
6. Koch, I.; Dee, J.; House, K.; Sui, J.; Zhang, J.; McKnight-Whitford, A.; Reimer, K.J. Bioaccessibility and speciation of arsenic in country foods from contaminated sites in Canada. *Sci. Total Environ.* **2013**, *449*, 1–8. [CrossRef]

7. Yang, J.M.; Liang, X.R.; Jiang, N.; Huang, Z.H.; Mou, F.L.; Zu, Y.Q.; Li, Y. Adsorption Characteristics of Modified Eucalyptus Sawdust for Cadmium and Arsenic and Its Potential for Soil Remediation. *Bull. Environ. Contam. Toxicol.* **2022**, *108*, 1056–1063. [CrossRef]
8. Zhang, K.; Yi, Y.Q.; Fang, Z.Q. Remediation of cadmium or arsenic contaminated water and soil by modified biochar: A review. *Chemosphere* **2023**, *311*, 136914. [CrossRef]
9. Yang, Z.H.; Gong, H.Y.; He, F.S.; Repo, E.; Yang, W.C.; Liao, Q.; Zhao, F.P. Iron-doped hydroxyapatite for the simultaneous remediation of lead-, cadmium- and arsenic-co-contaminated soil. *Environ. Pollut.* **2022**, *312*, 119953. [CrossRef]
10. Wei, M.; Chen, J.J.; Xia, C.H. Remediation of arsenic-cationic metals from smelter contaminated soil by washings of Na(2)EDTA and phosphoric acid: Removal efficiencies and mineral transformation. *Environ. Technol.* **2021**, *42*, 2211–2219. [CrossRef]
11. Lin, L.Y.; Zhu, R.L.; Li, Z.H.; Han, C.L.; Li, W.Y.; Deng, Y.R. A Combined Remediation Strategy of Arsenic and Cadmium in the Paddy Soil of Polymetallic Mining Areas. *Bull. Environ. Contam. Toxicol.* **2021**, *107*, 1220–1226. [CrossRef]
12. Gao, Y.Z.; Zhu, L.Z. Phytoremediation and its models for organic contaminated soils. *J. Environ. Sci.* **2003**, *15*, 302–310.
13. Lee, S.H.; Park, H.; Kim, J.G. Current Status of and Challenges for Phytoremediation as a Sustainable Environmental Management Plan for Abandoned Mine Areas in Korea. *Sustainability* **2023**, *15*, 2761. [CrossRef]
14. Marques, A.; Rangel, A.; Castro, P.M.L. Remediation of Heavy Metal Contaminated Soils: Phytoremediation as a Potentially Promising Clean-Up Technology. *Crit. Rev. Environ. Sci. Technol.* **2009**, *39*, 622–654. [CrossRef]
15. Bell, T.H.; Joly, S.; Pitre, F.E.; Yergeau, E. Increasing phytoremediation efficiency and reliability using novel omics approaches. *Trends Biotechnol.* **2014**, *32*, 271–280. [CrossRef] [PubMed]
16. Shi, P.; Fu, Y.H.; Li, Y. Study to identify potential hyper-accumulator plants suitable for phytoremediation of a copper and zinc mining wasteland in a cold region of northeastern china. *Fresenius Environ. Bull.* **2015**, *24*, 4344–4352.
17. Yu, F.M.; Tang, S.T.; Shi, X.W.; Liang, X.; Liu, K.H.; Huang, Y.Z.; Li, Y. Phytoextraction of metal(loid)s from contaminated soils by six plant species: A field study. *Sci. Total Environ.* **2022**, *804*, 150282. [CrossRef]
18. Yadav, R.; Singh, G.; Santal, A.R.; Singh, N.P. Omics approaches in effective selection and generation of potential plants for phytoremediation of heavy metal from contaminated resources. *J. Environ. Manag.* **2023**, *336*, 117730. [CrossRef]
19. Escobar-Alvarado, L.F.; Vaca-Mier, M.; Lopez, R.; Rojas-Valencia, M.N. Hydrocarbon Degradation and Lead Solubility in a Soil Polluted with Lead and Used Motor Oil Treated by Composting and Phytoremediation. *Bull. Environ. Contam. Toxicol.* **2018**, *100*, 280–285. [CrossRef]
20. Zha, F.S.; Ji, C.J.; Xu, L.; Kang, B.; Yang, C.B.; Chu, C.F. Assessment of strength and leaching characteristics of heavy metal-contaminated soils solidified/stabilized by cement/fly ash. *Environ. Sci. Pollut. Res.* **2019**, *26*, 30206–30219. [CrossRef]
21. Zhu, Q.H.; Wu, J.; Wang, L.L.; Yang, G.; Zhang, X.H. Effect of Biochar on Heavy Metal Speciation of Paddy Soil. *Water Air Soil Pollut.* **2015**, *226*, 429. [CrossRef]
22. He, X.M.; Zhang, J.; Ren, Y.N.; Sun, C.Y.; Deng, X.P.; Qian, M.; Hu, Z.B.; Li, R.; Chen, Y.H.; Shen, Z.G.; et al. Polyaspartate and liquid amino acid fertilizer are appropriate alternatives for promoting the phytoextraction of cadmium and lead in *Solanum nigrum* L. *Chemosphere* **2019**, *237*, 124483. [CrossRef] [PubMed]
23. Guo, J. Study on Heavy Metal Contaminated Soil in E-waste Dismantling Site Combined with Sludge High-temperature Treatment Residue and Plants. Master's Thesis, Shanghai Polytechnic University, Shanghai, China, 2022.
24. Wu, J.M.; Zhang, C.X.; Yang, H.F.; Chen, P.; Cao, J. Combined Remediation Effects of Pioneer Plants and Solid Waste towards Cd- and As-Contaminated Farmland Soil. *Appl. Sci.* **2023**, *13*, 5695. [CrossRef]
25. El Fadili, H.; Ben Ali, M.; Touach, N.; El Mahi, M.; Mostapha Lotfi, E. Ecotoxicological and pre-remedial risk assessment of heavy metals in municipal solid wastes dumpsite impacted soil in morocco. *Environ. Nanotechnol. Monit. Manag.* **2022**, *17*, 100640. [CrossRef]
26. Klik, B.; Holatko, J.; Jaskulska, I.; Gusiatin, M.Z.; Hammerschmiedt, T.; Brtnicky, M.; Liniauskiene, E.; Baltazar, T.; Jaskulski, D.; Kintl, A.; et al. Bentonite as a Functional Material Enhancing Phytostabilization of Post-Industrial Contaminated Soils with Heavy Metals. *Materials* **2022**, *15*, 8331. [CrossRef] [PubMed]
27. Chen, P.; Wu, J.M.; Li, L.; Yang, Y.H.; Cao, J. Modified fly ash as an effect adsorbent for simultaneous removal of heavy metal cations and anions in wastewater. *Appl. Surf. Sci.* **2023**, *624*, 157165. [CrossRef]
28. Kashem, M.A.; Singh, B.R. Metal availability in contaminated soils: I. Effects of flooding and organic matter on changes in Eh, pH and solubility of Cd, Ni andZn. *Nutr. Cycl. Agroecosyst.* **2001**, *61*, 247–255. [CrossRef]
29. Liu, Y.X.; Zeng, F.G.; Sun, B.L.; Jia, P. Research on XRD and FTIR Spectra of Fly Ash in Different Particle Size from Gujiao Power Plant. *Spectrosc. Spectr. Anal.* **2020**, *40*, 1452–1456. [CrossRef]
30. Liu, J.A.; Wang, J.; Chen, Y.H.; Lippold, H.; Lippmann-Pipke, J. Comparative characterization of two natural humic acids in the Pearl River Basin, China and their environmental implications. *J. Environ. Sci.* **2010**, *22*, 1695–1702. [CrossRef]
31. Pei, J.C.; Fan, L.W.; Xie, H. Study on the Vibrational Spectra and XRD Characters of Huanglong Jade from Longling County, Yunnan Province. *Spectrosc. Spectr. Anal.* **2014**, *34*, 3411–3414. [CrossRef]
32. Kannan, R.; Jegan, A.; Ramasubbu, A.; Karunakaran, K.; Vasanthkumar, S. Synthesis and catalytic stuides of layered and oms type nano manganese oxide material. *Dig. J. Nanomater. Biostruct.* **2011**, *6*, 755–760.
33. Montoya, A.; Reyes, J.L.; Reyes, I.A.; Cruz, R.; Lazaro, I.; Rodriguez, I. Effect of sodium hypochlorite as a depressant for copper species in Cu-Mo flotation separation. *Miner. Eng.* **2023**, *201*, 108166. [CrossRef]

34. Kong, H.S.; Kim, B.J.; Kang, K.S. Enhancement of Fire Retardancy Using Surface-Modified Silica Spheres with Aluminum Hydroxide. *Arab. J. Sci. Eng.* **2017**, *42*, 4473–4477. [CrossRef]
35. Xie, J.; Wu, S.P.; Pang, L.; Lin, J.T.; Zhu, Z.H. Influence of surface treated fly ash with coupling agent on asphalt mixture moisture damage. *Constr. Build. Mater.* **2012**, *30*, 340–346. [CrossRef]
36. Chelike, D.K.; Alagumalai, A.; Acharya, J.; Kumar, P.; Sarkar, K.; Thangavelu, S.A.G.; Chandrasekhar, V. Functionalized iron oxide nanoparticles conjugate of multi-anchored Schiff's base inorganic heterocyclic pendant groups: Cytotoxicity studies. *Appl. Surf. Sci.* **2020**, *501*, 143963. [CrossRef]
37. Abd Malek, N.N.; Jawad, A.H.; Abdulhameed, A.S.; Ismail, K.; Hameed, B.H. New magnetic Schiffs base-chitosan-glyoxal/fly ash/Fe_3O_4 biocomposite for the removal of anionic azo dye: An optimized process. *Int. J. Biol. Macromol.* **2020**, *146*, 530–539. [CrossRef]
38. Madejova, J.; Keckes, J.; Palkova, H.; Komadel, P. Identification of components in smectite/kaolinite mixtures. *Clay Min.* **2002**, *37*, 377–388. [CrossRef]
39. Chamling, P.K.; Haldar, S.; Patra, S. Physico-Chemical and Mechanical Characterization of Steel Slag as Railway Ballast. *Indian Geotech. J.* **2020**, *50*, 267–275. [CrossRef]
40. Chen, G.; Ling, Y.Q.; Li, Q.N.; Zheng, H.; Jiang, Q.; Li, K.Q.; Chen, J.; Peng, J.H.; Gao, L.; Omran, M.; et al. Investigation on microwave carbothermal reduction behavior of low-grade pyrolusite. *J. Mater. Res. Technol.* **2020**, *9*, 7862–7869. [CrossRef]
41. Jiang, Q.; He, Y.M.; Wu, Y.L.; Dian, B.; Zhang, J.L.; Li, T.G.; Jiang, M. Stabilization/stabilization of soil heavy metals by alkaline industrial wastes: A critical review. *Environ. Pollut.* **2022**, *312*, 120094. [CrossRef]
42. Liu, M.H.; Xia, Y.; Zhao, Y.D.; Chi, X.F.; Du, J.X.; Du, D.H.; Guo, J.Z.; Cao, Z.G. Na_2SO_4 modified low-carbon cementitious binder containing commercial low-reactivity metakaolin for heavy metal immobilization: Mechanism of physical encapsulation and chemical binding. *J. Build. Eng.* **2022**, *60*, 105194. [CrossRef]
43. Wang, X.J.; Wang, K.; Li, J.W.; Wang, W.L.; Mao, Y.P.; Wu, S.; Yang, S.Z. Heavy metals migration during the preparation and hydration of an eco-friendly steel slag-based cementitious material. *J. Clean Prod.* **2021**, *329*, 129715. [CrossRef]
44. Wang, S.T.; Dong, Q.; Wang, Z.L. Differential effects of citric acid on cadmium uptake and accumulation between tall fescue and Kentucky bluegrass. *Ecotox. Environ. Saf.* **2017**, *145*, 200–206. [CrossRef] [PubMed]
45. Lin, L.N.; Zhou, S.W.; Huang, Q.; Huang, Y.C.; Qiu, W.W.; Song, Z.G. Capacity and mechanism of arsenic adsorption on red soil supplemented with ferromanganese oxide-biochar composites. *Environ. Sci. Pollut. Res.* **2018**, *25*, 20116–20124. [CrossRef]
46. Ma, L.; Cai, D.M.; Tu, S.X. Arsenite simultaneous sorption and oxidation by natural ferruginous manganese ores with various ratios of Mn/Fe. *Chem. Eng. J.* **2020**, *382*, 123040. [CrossRef]
47. Frau, F.; Rossi, A.; Ardau, C.; Biddau, R.; Da Pelo, S.; Atzei, D.; Licheri, C.; Cannas, C.; Capitani, G. Determination of arsenic speciation in complex environmental samples by the combined use of TEM and XPS. *Microchim. Acta* **2005**, *151*, 189–201. [CrossRef]
48. Zhu, J.F.; Gao, W.C.; Zhao, W.T.; Ge, L.; Zhu, T.; Zhang, G.H.; Niu, Y.H. Wood vinegar enhances humic acid-based remediation material to solidify Pb(II) for metal-contaminated soil. *Environ. Sci. Pollut. Res.* **2021**, *28*, 12648–12658. [CrossRef]
49. Yamashita, T.; Hayes, P. Analysis of XPS spectra of Fe^{2+} and Fe^{3+} ions in oxide materials. *Appl. Surf. Sci.* **2008**, *254*, 2441–2449. [CrossRef]
50. Rao, X.F.; Lou, Y.T.; Zhao, J.J.; Chen, J.; Qiu, Y.P.; Wu, T.T.; Zhong, S.W.; Wang, H.; Wu, L.J. Carbon nanofibers derived from carbonization of electrospinning polyacrylonitrile (PAN) as high performance anode material for lithium ion batteries. *J. Porous Mat.* **2023**, *30*, 403–419. [CrossRef]
51. Xu, W.; Lan, H.C.; Wang, H.J.; Liu, H.M.; Qu, J.H. Comparing the adsorption behaviors of Cd, Cu and Pb from water onto Fe-Mn binary oxide, MnO_2 and FeOOH. *Front. Environ. Sci. Eng.* **2015**, *9*, 385–393. [CrossRef]